AGU PUBLICATIONS

Geophysical Research Letters

RESEARCH LETTER

10.1002/2017GL076410

Key Points:
- Linkage of sulfur source gases and remotely sensed aerosol numbers
- Western tropical Indian Ocean DMS hot spot confirmed
- First eddy covariance measurements of DMS in the Western Tropical Indian Ocean

Supporting Information:
- Supporting Information S1

Correspondence to:
A. Zavarsky,
alexz@mailbox.org

Citation:
Zavarsky, A., Booge, D., Fiehn, A., Krüger, K., Atlas, E., & Marandino, C. (2018). The influence of air-sea fluxes on atmospheric aerosols during the summer monsoon over the tropical Indian Ocean. *Geophysical Research Letters*, *45*. https://doi.org/10.1002/2017GL076410

Received 15 NOV 2017
Accepted 18 DEC 2017
Accepted article online 21 DEC 2017

The Influence of Air-Sea Fluxes on Atmospheric Aerosols During the Summer Monsoon Over the Tropical Indian Ocean

Alex Zavarsky[1], Dennis Booge[1], Alina Fiehn[1,2], Kirstin Krüger[2], Elliot Atlas[3], and Christa Marandino[1]

[1]GEOMAR Helmholtz Centre for Ocean Research Kiel, Kiel, Germany, [2]Department of Geosciences, University of Oslo, Oslo, Norway, [3]Rosenstiel School for Marine and Atmospheric Sciences, Miami, FL, USA

Abstract During the summer monsoon, the western tropical Indian Ocean is predicted to be a hot spot for dimethylsulfide emissions, the major marine sulfur source to the atmosphere, and an important aerosol precursor. Other aerosol relevant fluxes, such as isoprene and sea spray, should also be enhanced, due to the steady strong winds during the monsoon. Marine air masses dominate the area during the summer monsoon, excluding the influence of continentally derived pollutants. During the SO234-2/235 cruise in the western tropical Indian Ocean from July to August 2014, directly measured eddy covariance DMS fluxes confirm that the area is a large source of sulfur to the atmosphere (cruise average 9.1 μmol m^{-2} d^{-1}). The directly measured fluxes, as well as computed isoprene and sea spray fluxes, were combined with FLEXPART backward and forward trajectories to track the emissions in space and time. The fluxes show a significant positive correlation with aerosol data from the Terra and Suomi-NPP satellites, indicating a local influence of marine emissions on atmospheric aerosol numbers.

Plain Language Summary The air-sea flux trace gases and their transformation to aerosols and cloud condensation nuclei may be fundamental to cloud formation in the marine environment. Clouds and aerosol have an important influence on the radiative balance of the earth. The local coupling of air-sea fluxes and the formation of aerosols and clouds over the ocean is still highly uncertain. This study combines directly measured air-sea fluxes with satellite aerosol remote sensing. It is a novel, interdisciplinary approach where results from air-sea gas transfer are combined with atmospheric chemistry satellite remote sensing using meteorological transport models. Our results strongly support a local influence of marine-derived aerosol precursors on cloud condensation nuclei and aerosol optical depth above the tropical Indian Ocean.

1. Introduction

The CLAW hypothesis (Charlson et al., 1987), still heavily debated in the scientific community (Quinn & Bates, 2011), describes a feedback process connecting oceanic production to cloud formation, which influences Earth's albedo and as a consequence oceanic production. One of the main steps of the CLAW hypothesis is the formation of aerosols and cloud condensation nuclei (CCN) in the marine boundary layer (MBL). The original publication proposed dimethylsulfide (DMS) to be the key source of CCN and driver of the feedback. DMS is produced by phytoplankton in the ocean and then released into the atmosphere, where it is one of the major sulfur sources (Quinn & Bates, 2011). In the atmosphere it undergoes oxidation to sulfur dioxide, sulfuric acid, or methane sulfonic acid and subsequently forms CCN. In more recent years other CCN sources, for instance sea spray and other biogenic trace gases such as isoprene, have come into focus. Quinn and Bates (2011) argue that only 40–50% of the MBL-CCN can be attributed to sulfur emissions and, depending on the region, up to 65% can be attributed to sea salt aerosols. For the tropics the sea spray contributions decrease to 30% (Quinn et al., 2017). The quantitative impact of isoprene is still unclear. Furthermore, Quinn and Bates (2011) and Quinn et al. (2017) claim that most of the DMS derived CCN are actually formed in the free troposphere and then entrained into the boundary layer again. This would mean a regional decoupling of the DMS emissions and the formation of clouds, which is in opposition to the CLAW feedback. As pointed out by Vallina et al. (2006) and Green and Hatton (2014) most studies lack the temporal and spatial coverage to give a significant answer to the importance of DMS in the CCN forming process in the MBL. In contrast to the arguments of Quinn and Bates (2011), Lana et al. (2012) performed a satellite-based correlation study,

connecting DMS and sea spray fluxes (SSPFs) with satellite-derived CCN number concentrations. They found a rather uniform positive correlation for DMS-CCN (with some areas of weak correlation at the boundaries of the tropics). For sea spray-CCN the correlation depended on latitude: The tropics exhibited a positive correlation, the northern midlatitudes exhibited a negative correlation, and the southern midlatitudes exhibited a mixed correlation. These findings provide a basis for further investigation, but no studies have correlated air-sea fluxes with aerosol numbers on a regional level or multiday time scales.

According to the Lana climatology (Lana et al., 2011), the western tropical Indian Ocean (WTIO) is a hot spot for DMS flux during the months July and August. The efflux is one of the highest worldwide (63.32 μmol m^{-2} d^{-1}). The WTIO is associated with marine-influenced air masses during the boreal summer (Rhoads et al., 1997). Biological productivity, especially in the upwelling areas of the WTIO (off north east Africa and the north Arabian Sea), is strongly correlated with the monsoon seasonal cycle (Yoder et al., 1993). This production influences the DMS concentration in the surface water and, together with steady strong winds, enhances gas transfer.

Thus, the WTIO could be an important source of sulfur to the atmosphere, and the SO234-2/235 cruise provides the opportunity to study the DMS-aerosol connection. We focus on linking source gases and aerosol numbers in order to evaluate the Lana et al. (2012) correlations. We use an improved approach, as our DMS fluxes were directly measured and coupled to the atmospheric transport model FLEXPART to study atmospheric sulfur transformations on a regional scale above the WTIO. Thus, the WTIO could be an important source of sulfur to the atmosphere, and the SO234-2/235 cruise provides the opportunity to study the DMS-aerosol connection. We focus on linking source gases and aerosol numbers in order to evaluate the Lana et al. (2012) correlations. We use an improved approach, as our DMS fluxes were directly measured and coupled to the atmospheric transport model FLEXPART to study atmospheric sulfur transformations on a regional scale above the WTIO.

2. Methods

We performed direct eddy covariance DMS flux measurements aboard the RV Sonne sailing from Durban, SA, to Port Louis, MU (SO234-2, 8–20 July 2014) and from Port Louis, MU, to Malé, MV (SO235, 23 July to 8 August 2014) (Figure 1). Additionally, we measured DMS and isoprene surface water and air concentrations. Basic meteorological observations were done by the ship's weather station. For the span of the cruise, backward and forward trajectories were calculated using the FLEXPART model (Stohl et al., 2005) with ERA-interim reanalysis (Figure 2). Aerosol satellite data from the Terra and Suomi-NPP satellites were acquired for the area and time covered by the cruise track and the trajectories.

2.1. Eddy Covariance Measurements

The eddy covariance flux F (equation (1)) is a product of the dry air density (ρ), the fluctuation of vertical wind speed (w′), and the fluctuation of the mixing ratio (c′).

$$F = \rho \cdot c'w' \tag{1}$$

We recorded DMS air mixing ratios at 5 Hz using an atmospheric pressure chemical ionization mass spectrometer (AP-CIMS) similar to that described by Saltzman et al. (2009). The air was sampled from a mast at the bow of the ship (11 m above sea level) and pumped at 50–70 L min^{-1} ($Flow_{total}$) through a 1/2″ diameter and 25 m long polytetrafluoroethylene tube to a laboratory container where the AP-CIMS was placed. The air stream was dried using a Nafion membrane (Perma Pure) prior to analysis. For calibration, we continuously added a deuterated DMS standard (DMS-d3, 2.28 ppm C_{tank}) to the inlet at the rate of 2 mL min^{-1} ($Flow_{std}$). Using the ratio of the deuterated DMS counts ($Counts_{66}$) to the natural DMS counts ($Counts_{63}$), the concentration of atmospheric DMS (DMS_{air}) was calculated:

$$DMS_{air} = \frac{Flow_{std}}{Flow_{total}} \cdot \frac{Counts_{63}}{Counts_{66}} \cdot C_{tank} \tag{2}$$

Two ultrasonic anemometers (CSAT3), mounted next to the air-sample inlet, measured the 3-D turbulent wind field. We determined the delay, between the passage of the air parcel at the inlet and the measurement at the AP-CIMS, with a valve switch before each 1 h eddy covariance measurement run. A GPS and an inertial measurement unit (Landmark 10), positioned next to the sonic anemometers provided the data for the motion correction of the 3-D wind, which we performed based on Edson et al. (1998) and Miller et al. (2008), with an update by Landwehr et al. (2015). We recorded a total of 130.15 h DMS air measurements. The data set was split

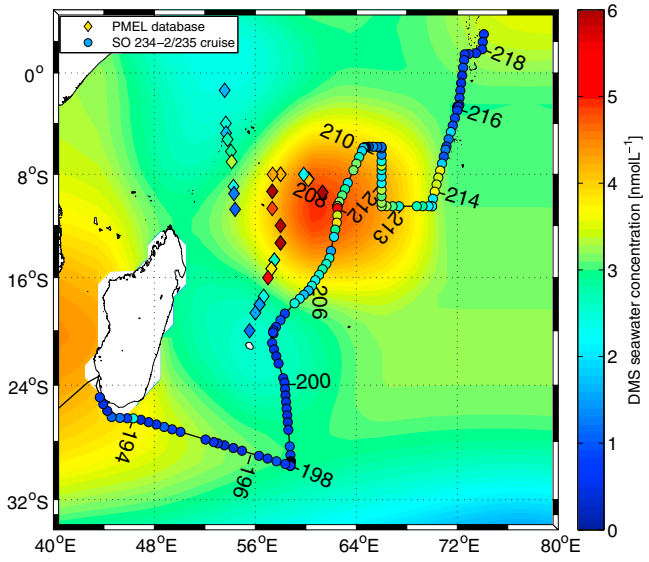

Figure 1. Cruise track (black solid line) of SO234-2/235. Circles are discrete sampled surface water DMS concentrations. Diamonds are all recorded DMS values within the PMEL database for July and August. July DMS surface concentrations from the Lana climatology are color coded in the background. The numbers indicate the day of year (DOY).

into 477 running intervals (10 min step), each 29.6 min long. These intervals fulfilled the flow distortion relative wind direction criterion of ±90° from the bow and the Landwehr requirement of steady wind direction.

2.2. Bulk Air and Seawater Measurements

Seawater DMS and isoprene concentrations were measured using a purge and trap system attached to a gas chromatograph/mass spectrometer (GC/MS; Agilent 7890A/Agilent 5975C). We sampled the water from a constant stream out of the ship's moon pool at 5 m depth and measured within 15 min of collection. The gases were purged from the water sample for 15 min and then dried using potassium carbonate. The dried gas was preconcentrated in a trap cooled with liquid nitrogen and injected into the GC. We obtained a total of 162 DMS and isoprene sea surface concentration values (3 h sampling interval). At the same time and interval, we filled stainless steel canisters with air samples (25 m sampling height), which were analyzed for more than fifty gases, including DMS and isoprene, at the University of Miami.

We calculated isoprene fluxes using the bulk method (equation (3)), where c_a and c_w are the respective air and water concentrations, H is the dimensionless form of Henry's law constant and k the gas transfer velocity by Nightingale et al. (2000). This parameterization was used, because direct flux CO_2 measurements show a k versus wind speed relationship following Nightingale et al. (2000). CO_2 and isoprene have approximately the same solubility.

$$\text{Flux} = k \cdot \left(c_w - \frac{c_a}{H} \right) \tag{3}$$

SSPF (F_{seaspray}, billion particles ejected per m^2 per day, Gpart m^{-2} d^{-1}) was parameterized using equation (4), which was proposed by O'Dowd et al. (2008). The wind speed at 22 m (u_{22}) was calculated using the parameterization by Hsu et al. (1994).

$$F_{\text{seaspray}} = 1.854 \cdot 10^{-3} \cdot u_{22}^{2.706} \tag{4}$$

2.3. Backward and Forward Trajectories

For the trajectory calculations, we used the Lagrangian Particle Dispersion Model FLEXPART Version 9.2 (Stohl et al., 2005). The model includes moist convection and turbulence parameterizations in the atmospheric

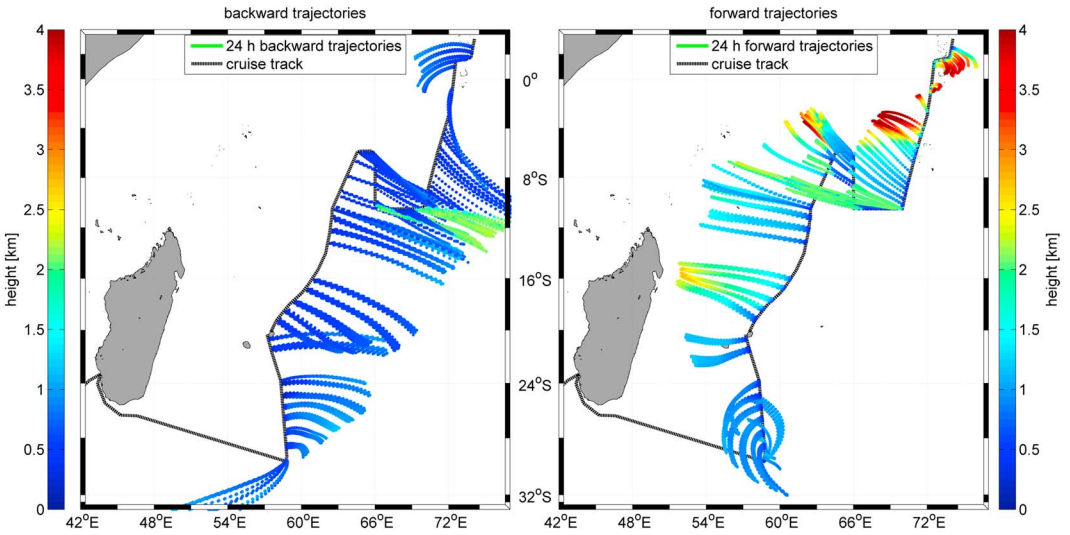

Figure 2. (left) Backward trajectories; (right) forward trajectories (24 h) calculated using FLEXPART/ERA-Interim. The color is showing the average height of the trajectory. In total 435 backward and forward trajectories are shown. For the correlation calculation forward (downwind) trajectories up to 12 h were used.

boundary layer and free troposphere (Forster et al., 2007; Stohl & Thomson, 1999). We used FLEXPART with the European Centre for Medium-Range Weather Forecasts reanalysis product ERA-Interim (Dee et al., 2011) with a horizontal resolution of 1° × 1° and 60 vertical model levels as meteorological input fields with a 6 hourly temporal resolution. During the cruise we launched radiosondes to improve meteorological reanalysis (e.g., ERA-Interim) for the later use in the transport model (Fiehn et al., 2017). FLEXPART was run with a synchronization interval of 900 s and with a quarter of this time step in the atmospheric boundary layer to resolve turbulent fluxes on short time scales. The model output was recorded hourly. An ensemble of 10,000 forward and 1,000 backward trajectories are started at the positions and times of the 435 direct DMS flux measurements and run for 10 days. From the hourly trajectory positions we calculated the mean trajectory as an average of all ensemble members. Trajectories reaching 12 h backward and 12 h forward were used in the correlation calculation (Figure 2). Longer time spans up to 10 days were used to assess the possible influence of terrestrial pollution (Figure S1).

2.4. Remote Sensing

We obtained total column CCN and aerosol optical depth (AOD) data (Level 3, Moderate Resolution Imaging Spectroradiometer (MODIS)-Terra 6 collection, Hubanks et al., 2016), provided on a global 1° × 1° grid, from the MODIS instrument on board the Terra satellite. Terra has a sun synchronous orbit and an overpass at 10:30 local time. Additionally, total column aerosol optical thickness (AOT) was obtained from the Visible Infrared Imaging Radiometer Suite instrument on board the Suomi-NPP satellite, which has a sun synchronous orbit and an overpass at 13:30 local time. The level-2 aerosol product has a resolution of 0.25° × 0.25°. AOD and AOT both describe the degree to which aerosols prevent the transmission of light by absorption or scattering of light. In total we obtained daily files from 27 June 2014 to 19 August 2014 for all products. The output describes the aerosol properties at the time of the overpass. Using two different satellites gives the opportunity to test the data with two independent systems. A cross-check was done between the Aqua, Terra, and NPP-Suomi satellites, which shows consistent results (data shown in the supporting information).

The satellite data were linearly interpolated to the specific location of each forward and backward trajectory output. If, due to missing values, the first interpolation was not successful, following steps were carried out successively and stopped if one interpolation returned a valid result: (1) a nearest interpolation (space and time), (2) linear interpolation (space, at closest time step), and (3) mean of nearest-neighbors (space, at closest time step). The majority of missing values were caused by clouds. An error estimation of the satellite data is presented in the supporting information (Table S14, (Huang et al., 2016; Levy et al., 2013; Rosenfeld et al., 2016).

2.5. Correlation

To link the oceanic sources to the aerosol numbers, we analyze the trend of the aerosol properties in the downwind (forward trajectories) area. This approach has already been established for volcanoes (Eguchi et al., 2011; Mace & Abernathy, 2016; Yuan et al., 2011) and focuses on the absolute aerosol number or cloud density. We have extended their method, and, instead of a single point source (volcano), we correlate multiple point sources, all measured fluxes from the cruise track, with the satellite aerosol properties in the downwind area. We hypothesize that a higher efflux of aerosol precursor, such as DMS, isoprene, and sea spray, should lead to a higher value of satellite sensed aerosol numbers. Therefore, a positive correlation between aerosol predecessor and aerosol number should be observed. We calculated FLEXPART/ERA-Interim forward trajectories to pinpoint the downwind location of the directly measured fluxes. We used the locations from the time of the measurements until 12 h into the downwind area to obtain the satellite-based aerosol values. We averaged these values for every forward trajectory and then correlated them to the fluxes from the cruise track. The averaging along each trajectory provides a more representative picture of the aerosol numbers in the downwind area.

We used Spearman's rank as correlation method, which describes a monotonically increasing relationship between two independent variables. The bootstrap method was used to prove the level of significance. A correlation coefficient of 0.2 is statistically significant with a probability of 0.995. The 435 datapoints were correlated.

3. Results and Discussion

The cruise took place during the Asian summer monsoon season, with prevailing southeasterly winds south of the Equator and southwesterly winds north of the Equator. The SO234-2/235 cruise track spanned a range

of oceanic areas, traversing the Agulhas current, the Antarctic circumpolar current (an area of high carbon dioxide drawdown), the Indian Ocean Gyre, the South Equatorial Current, the Equatorial Countercurrent, and the North Equatorial Current. Shallow areas (e.g., the Mascarene Plateau) and reef areas (e.g., Maldives) were also traversed. We encountered an average oceanic mixed layer depth of 60 m, sea surface temperatures from 19°C to 25°C, practical salinity from 34 to 36 and generally low nutrient levels (below 0.1 μmol L^{-1} for nitrate and below 0.2 μmol L^{-1} for phosphate). Some areas of enhanced nutrients were encountered between 10° and 5°S. Chlorophyll levels were between 0.05 and 0.59 μg L^{-1} with a mean of 0.23 μg L^{-1}. During the first leg (SO234-2), 30 min averaged wind speed below 10 m s^{-1} was measured. North of Mauritius the wind speed increased to a maximum of 16 m s^{-1} and then gradually declined toward the Maldives. Lower wind speed prevailed closer to the Equator, which is in agreement with the monsoon circulation. The average MBL height was 0.8 km, determined by radiosonde soundings applying a threshold of the critical Richardson number of Ric = 0.25 (Fiehn et al., 2017). The relative humidity varied between 50% and 90%, and air temperatures ranged between 14°C and 30°C (Fiehn et al., 2017). Precipitation was variable over the cruise tracks. Generally, the air masses encountered were unpolluted and originated from over the ocean (Figure 2). This is supported by 10 day backward trajectories and profiles from ozone sonde soundings, where averaged cruise values reveal low tropospheric ozone values (22 ppb near the surface, 26 ppb at 1 km, and 51 ppb at 5 km) (Figures S1 and S2).

3.1. Seawater Concentrations

Measured DMS surface seawater concentrations ranged from 0.4 to 5.19 nmol L^{-1} (Figure 3). During the first leg (SO234-2), the concentrations stayed below 1.4 nmol L^{-1}, with one exception of 2.4 nmol L^{-1} at the southern tip of Madagascar, where a shallow biological productive area (Banc d'Etoile) was crossed. DMS values started increasing up to the maximum value of 5.19 nmol L^{-1} north of Mauritius in the area between 18° S and 5° S. Further north, the values declined to sub 1 nmol L^{-1} levels. Two main features influenced the DMS values north of Mauritius: (1) The Mascarene Plateau (between 55/65° E;5/20° S) (Smythe-Wright et al., 2005), which is an extensive submarine plateau reaching a shallowness of up to 50 m. (2) As described by Schott et al. (2009), during both monsoon seasons a southward Ekman transport subducts underneath the equatorial roll. This leads to upwelling south of this roll in the area between 10° S and 6° S, which elevates biological productivity and, as a result, also the production of biogenically produced trace gases.

Isoprene water concentrations ranged from 0.36 pmol L^{-1} to a maximum of 64 nmol L^{-1} (Figure 3). During SO234-2, from Durban to Mauritius, average values around 10 pmol L^{-1} were observed. North of Mauritius the isoprene concentration steadily increased from sub 1 nmol L^{-1} just off Mauritius to around 30 pmol L^{-1} at the Maldives. The maximum values of isoprene were reached at 6.1° S and 64.45° E on day of year 2014 (DOY) 209.45 (Booge et al., 2016). The DMS and isoprene seawater distributions were anticorrelated over most of the cruise tracks.

3.2. Fluxes

Directly measured DMS fluxes ranged from 0.3 to 32.77 μmol m^{-2} d^{-1} (Figure 3). During SO234-2 from Durban to Mauritius and after DOY 214 the fluxes were low, which can be attributed to low wind speed (below 10 m s^{-1}) and low water concentrations. After Mauritius at DOY 205 a high wind speed event (wind speed maximum of 16 m s^{-1}) was encountered. High wind speed in conjunction with high seawater concentrations were measured, leading to an increase of the flux. Wind speed steadily decreased as the cruise continued, but seawater concentrations varied, causing the fluxes to vary accordingly in magnitude from DOY 210 onward. The lowest fluxes occurred on DOY 198 and the highest on DOY 207. Isoprene fluxes ranged from 0 to 0.187 μmol m^{-2} d^{-1}. Generally, the isoprene fluxes of SO235 were higher, which is associated for the most part with the higher wind speed and second with the slightly higher water concentrations. The computed SSPF closely resembles the measured wind speed (Figure 3).

3.3. Comparison to the Lana Climatology and PMEL Database

Generally, the sea surface DMS concentrations throughout the cruise legs are lower than those published in the Lana climatology (Lana et al., 2012) and the PMEL (NOAA Pacific Marine Environmental Laboratory) database (Figure 1) (Kettle et al., 1999). A description of the Lana climatology and the PMEL database can be found in the supporting information. The WTIO is heavily undersampled, especially in the months July and August. The only data available, and therefore used, in the Lana climatology are 34 samples from two cruises (Mihalopoulos et al., 1992; Smythe-Wright et al., 2005) (Diamonds, Figure 1). The influence of the Mascarene Plateau on biological productivity might be the reason for the general elevated DMS concentrations from

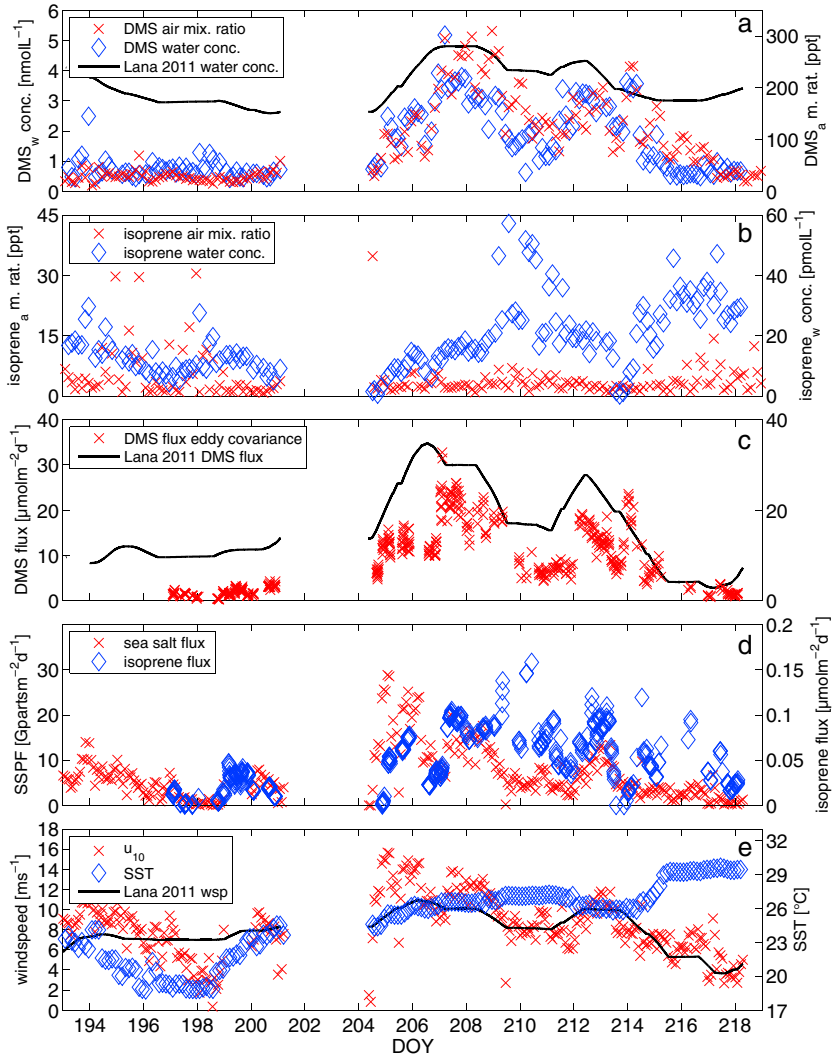

Figure 3. Time series along the cruise track (*x* axis DOY 2014), (a) DMS surface seawater concentration (diamonds) and the air mixing ratio (crosses), (b) isoprene surface water concentrations (diamonds) and air mixing ratios (crosses), (c) the measured DMS flux (crosses) and Lana's climatological DMS flux (line), (d) isoprene flux and SSPF, and (e) sea surface temperature (diamonds) and u_{10} along the cruise track, measured (crosses) and used by the Lana climatology (line). The error estimates are the following: DMS_{air} 5%, DMS_{water} 10%, $Isoprene_{air}$ 5%, $Isoprene_{water}$ 10%, and Eddy Covariance 25% (Edson et al., 1998; Marandino et al., 2007)

both the PMEL database and the Lana climatology (background Figure 1). As the database's seawater concentrations were measured farther west than our cruise track, they were located more directly in the region impacted by the Mascarene Plateau and values up to 9 nmol L^{-1} were incorporated in the climatology. Our highest measure value was 5.19 nmol L^{-1}.

On a global scale the WTIO represents the DMS flux hot spot for July. Our maximum value of 32.77 µmol m^{-2} d^{-1} is of the same magnitude as the worldwide maximum value (31.8 µmol m^{-2} d^{-1}), excluding the Indian Ocean (IO). The maximum value of the IO from the Lana climatology is 63.2 µmol m^{-2} d^{-1} and is twice as much as measured during our cruise. Although larger than our measurements, this value is still plausible because it is located at 10° S 59° E and therefore more directly influenced by the Mascarene Plateau. This supports the importance of the IO as a source of DMS during this season. Fluxes computed from the Lana climatology corresponding to our cruise location and dates range between 2.22 and 34.78 µmol m^{-2} d^{-1} (this study 0.3–32.77 µmol m^{-2} d^{-1}). On average, Lana's predicted fluxes are 60% higher (Lana mean: 14.9 µmol m^{-2} d^{-1}, this study mean: 9.1 µmol m^{-2} d^{-1}, Figure 3). The reason for these differences is twofold. (1) The Lana climatology uses higher DMS seawater concentrations than those we measured in situ.

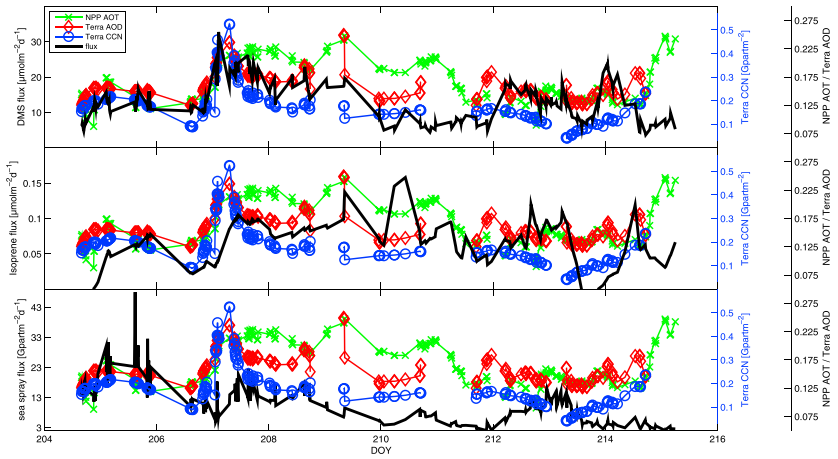

Figure 4. Time series of DMS flux (top), isoprene flux (middle) and SSPF (bottom) from DOY 204.66 to 215.25 shown together with the data from the Terra satellite (Terra-CCN and Terra-AOD) and the NPP satellite (NPP-AOT). The aerosol products shown are the average along the forward trajectory from the time of the flux measurement until 12 h. Uncertainty estimates are shown in the supporting information.

(2) The air-sea flux parameterization (equation (3)) used in the climatology (Nightingale et al., 2000) has a quadratic dependence of the gas transfer velocity k on wind speed. However, our directly measured fluxes and the associated gas transfer velocity appear to have a linear relationship to wind speed. As the wind speed experienced during the cruise and the wind speed used by the climatology were similar (Figure 3), the difference in a quadratic and a linear dependence resulted in an increase of the Lana DMS flux.

3.4. Correlations With Aerosol Properties

Figure 4 shows a time series of the fluxes at the cruise track. Overlaid are the averaged satellite data from the downwind area. The averaging was done from the time of the flux measurement until 12 h into the forward trajectory. The largest fluxes of DMS, in the top panel, are around DOY 207-208. Additionally, at DOY 212-214, a secondary maximum, followed by a short decrease and sudden increase, can be seen. Similar characteristics are visible in all three satellite products. For isoprene, the highest fluxes occurred at DOY 209–211. Similar to DMS fluxes, the isoprene fluxes at the end of the cruise increase, decrease, and then sharply increase again. CCN and AOD seem to roughly follow this feature. This is reflected in the correlation coefficients: DMS-CCN 0.425, DMS-AOD 0.625, Isoprene-AOD 0.4, and Isoprene-AOT 0.43.

SSPF has its main feature at DOY 205, when the wind speed was highest and steadily decreases over the cruise track. The Terra CCN product distribution follows the SSPF source distribution, whereas the other aerosol satellite product distributions do not appear similar to the trend of the SSPF distribution. This is supported by the correlation coefficients: SSPF-CCN 0.49, SSPF-AOD 0.16, and SSPF-AOT -0.04

All three fluxes in Figure 4 have distinct features at different times, corresponding to different trends in the downwind aerosol product distributions. This allows us to qualitatively estimate the influence of each source on the satellite product. The aerosol product distribution more closely resembles the trace gas fluxes than the SSPF distributions. Nonetheless, there are also differences between the two trace gases, which are reflected in the aerosol product distributions. For example, the spatial distribution of the isoprene fluxes is anticorrelated with the DMS fluxes at DOY 212 and 214 and the maxima and minima are offset for the two trace gas fluxes. A second example is the isoprene flux trend from DOY 209–211, which is not well represented in the downwind satellite product distribution. The SSPF distribution, which starts high and then gradually decreases, does not seem to have great influence on the satellite aerosol product distribution, which does not mean that overall SSPF is not an aerosol precursor in this study region. This is supported by Quinn et al. (2017) who find a 30% contribution of SSPF to the CCN budget in the tropics. As quality control, we correlated the fluxes with the backward (upwind) trajectories up to −12 h. These correlations are insignificant or negative. The full collection of correlations and the full comparison of flux data and satellite data are shown in the supporting information (Figures S3–S6, Tables S7, and S8).

4. Conclusion

In this study, we observed that the WTIO during the summer monsoon period is one of the world's largest DMS source regions to the atmosphere. We correlated our directly measured DMS, as well as calculated isoprene fluxes and SSPF, with satellite-derived aerosol numbers over the IO during the summer monsoon. The maximum correlations including regional transport, computed using trajectories from the FLEXPART/ERA-Interim model, were statistically significant. These results illustrate the regional coupling between marine-derived precursors and aerosol products in the remote MBL. This is important, as regional coupling can give rise to local feedback processes. Although we acknowledge that correlation results do not always imply causation, the ensemble findings support the idea that marine-derived biogenic trace gases, as well as sea spray, influence the aerosol properties on a regional scale.

Acknowledgments
The authors thank the crew of the RV Sonne (SO234-2/235). Steffen Fuhlbrügge prepared and carried out the ozone sondes preparations and launches and helped with the postprocessing of the data. E. Atlas acknowledges support from the NASA UARP program and thanks Leslie Pope and Xiaorong Zhu for the canister preparation. The authors acknowledge NASA and NOAA for providing the satellite data. We thank the ECMWF for providing the ERA-Interim reanalysis data and the FLEXPART development team. This work was carried out under the Helmholtz Young Investigator Group of C. Marandino, TRASE-EC (VH-NG-819), from the Helmholtz Association. The cruise 234-2/235 and A. Fiehn were financed by the BMBF, 03G0235A. The authors declare no competing financial interests. The data are stored at the data portal of GEOMAR Kiel. Kirstin Krüger acknowledges financial support from the EU FP7 StratoClim project (603557).

References

Booge, D., Marandino, C. A., Schlundt, C., Palmer, P. I., Schlundt, M., Atlas, E. L., … Wallace, D. W. R. (2016). Can simple models predict large-scale surface ocean isoprene concentrations? *Atmospheric Chemistry and Physics*, *16*(18), 11,807–11,821. https://doi.org/10.5194/acp-16-11807-2016

Charlson, R. J., Lovelock, J. E., Andreae, M. O., & Warren, S. G. (1987). Oceanic phytoplankton, atmospheric sulphur, cloud albedo and climate. *Nature*, *326*(6114), 655–661. https://doi.org/10.1038/326655a0

Dee, D. P., Uppala, S. M., Simmons, A. J., Berrisford, P., Poli, P., Kobayashi, S., … Vitart, F. (2011). The ERA-Interim reanalysis: Configuration and performance of the data assimilation system. *Quarterly Journal of the Royal Meteorological Society*, *137*(656), 553–597. https://doi.org/10.1002/qj.828

Edson, J. B., Hinton, A. A., Prada, K. E., Hare, J. E., & Fairall, C. W. (1998). Direct covariance flux estimates from mobile platforms at sea. *Journal of Atmospheric and Oceanic Technology*, *15*(2), 547–562. https://doi.org/10.1175/1520-0426(1998)015<0547:dcfefm>2.0.co;2

Eguchi, K., Uno, I., Yumimoto, K., Takemura, T., Nakajima, T. Y., Uematsu, M., & Liu, Z. (2011). Modulation of cloud droplets and radiation over the North Pacific by sulfate aerosol erupted from Mount Kilauea. *SOLA*, *7*, 77–80. https://doi.org/10.2151/sola.2011-020

Fiehn, A., Quack, B., Hepach, H., Fuhlbrügge, S., Tegtmeier, S., Toohey, M., … Krüger, K. (2017). Delivery of halogenated very short-lived substances from the west indian ocean to the stratosphere during asian summer monsoon. *Atmospheric Chemistry and Physics Discussions*, *2017*, 1–40. https://doi.org/10.5194/acp-2017-8

Forster, C., Stohl, A., & Seibert, P. (2007). Parameterization of convective transport in a lagrangian particle dispersion model and its evaluation. *Journal of Applied Meteorology and Climatology*, *46*(4), 403–422. https://doi.org/10.1175/jam2470.1

Green, T. K., & Hatton, A. D. (2014). *The CLAW hypothesis: A new perspective on the role of biogenic sulphur in the regulation of global climate* (pp. 315–336). Boca Raton, FL: Oceanography and Marine Biology - An Annual Review, CRC Press. https://doi.org/10.1201/b17143-7

Hsu, S. A., Meindl, E. A., & Gilhousen, D. B. (1994). Determining the power-law wind-profile exponent under near-neutral stability conditions at sea. *Journal of Applied Meteorology*, *33*(6), 757–765. https://doi.org/10.1175/1520-0450(1994)033<0757:dtplwp>2.0.co;2

Huang, J., Kondragunta, S., Laszlo, I., Liu, H., Remer, L. A., Zhang, H., … Petrenko, M. (2016). Validation and expected error estimation of suomi-npp viirs aerosol optical thickness and Angström exponent with aeronet. *Journal of Geophysical Research: Atmospheres*, *121*, 7139–7160. https://doi.org/10.1002/2016JD024834

Hubanks, P., Platnick, S., King, M., & Ridgway, B. (2016). Modis atmosphere l3 gridded product algorithm theoretical basis document for c6 (Tech. Rep. ATBD Reference Number: ATBD-MOD-30). NASA.

Kettle, A. J., Andreae, M. O., Amouroux, D., Andreae, T. W., Bates, T. S., Berresheim, H., … Uher, G. (1999). A global database of sea surface dimethylsulfide (DMS) measurements and a procedure to predict sea surface DMS as a function of latitude, longitude, and month. *Global Biogeochemical Cycles*, *13*(2), 399–444. https://doi.org/10.1029/1999GB900004

Lana, A., Bell, T. G., Simo, R., Vallina, S. M., Ballabrera-Poy, J., Kettle, A. J., … Liss, P. S. (2011). An updated climatology of surface dimethlysulfide concentrations and emission fluxes in the global ocean. *Global Biogeochemical Cycles*, *25*, GB1004. https://doi.org/10.1029/2010GB003850

Lana, A., Simo, R., Vallina, S. M., & Dachs, J. (2012). Potential for a biogenic influence on cloud microphysics over the ocean: A correlation study with satellite-derived data. *Atmospheric Chemistry and Physics*, *12*(17), 7977–7993. https://doi.org/10.5194/acp-12-7977-2012

Landwehr, S., O'Sullivan, N., & Ward, B. (2015). Direct flux measurements from mobile platforms at sea: Motion and airflow distortion corrections revisited. *Journal of Atmospheric and Oceanic Technology*, *32*(6), 1163–1178. https://doi.org/10.1175/jtech-d-14-00137.1

Levy, R. C., Mattoo, S., Munchak, L. A., Remer, L. A., Sayer, A. M., Patadia, F., & Hsu, N. C. (2013). The collection 6 MODIS aerosol products over land and ocean. *Atmospheric Measurement Techniques*, *6*(11), 2989–3034. https://doi.org/10.5194/amt-6-2989-2013

Mace, G. G., & Abernathy, A. C. (2016). Observational evidence for aerosol invigoration in shallow cumulus downstream of Mount Kilauea. *Geophysical Research Letters*, *43*, 2981–2988. https://doi.org/10.1002/2016GL067830

Marandino, C. A., De Bruyn, W. J., Miller, S. D., & Saltzman, E. S. (2007). Eddy correlation measurements of the air/sea flux of dimethylsulfide over the North Pacific Ocean. *Journal of Geophysical Research*, *112*, D03301. https://doi.org/10.1029/2006JD007293

Mihalopoulos, N., Nguyen, B. C., Putaud, J. P., & Belviso, S. (1992). The oceanic source of carbonyl sulfide (COS). *Atmospheric Environment. Part A. General Topics*, *26*(8), 1383–1394. https://doi.org/10.1016/0960-1686(92) 90123-3

Miller, S. D., Hristov, T. S., Edson, J. B., & Friehe, C. A. (2008). Platform motion effects on measurements of turbulence and air–sea exchange over the open ocean. *Journal of Atmospheric and Oceanic Technology*, *25*(9), 1683–1694. https://doi.org/10.1175/2008jtecho547.1

Nightingale, P. D., Malin, G., Law, C. S., Watson, A. J., Liss, P. S., Liddicoat, M. I., … Upstill-Goddard, R. C. (2000). In situ evaluation of air-sea gas exchange parameterizations using novel conservative and volatile tracers. *Global Biogeochemical Cycles*, *14*(1), 373–387. https://doi.org/10.1029/1999GB900091

O'Dowd, C. D., Langmann, B., Varghese, S., Scannell, C., Ceburnis, D., & Facchini, M. C. (2008). A combined organic-inorganic sea-spray source function. *Geophysical Research Letters*, *35*, L01801. https://doi.org/10.1029/2007GL030331

Quinn, P. K., & Bates, T. S. (2011). The case against climate regulation via oceanic phytoplankton sulphur emissions. *Nature*, *480*(7375), 51–56. https://doi.org/10.1038/nature10580

Quinn, P. K., Coffman, D. J., Johnson, J. E., Upchurch, L. M., & Bates, T. S. (2017). Small fraction of marine cloud condensation nuclei made up of sea spray aerosol. *Nature Geoscience*, *10*(9), 674–679.

Rhoads, K. P., Kelley, P., Dickerson, R. R., Carsey, T. P., Farmer, M., Savoie, D. L., & Prospero, J. M. (1997). Composition of the troposphere over the indian ocean during the monsoonal transition. *Journal of Geophysical Research*, *102*(D15), 18,981–18,995. https://doi.org/10.1029/97JD01078

Rosenfeld, D., Zheng, Y., Hashimshoni, E., Pohlker, M. L., Jefferson, A., Pohlker, C., … Andreae, M. O. (2016). Satellite retrieval of cloud condensation nuclei concentrations by using clouds as CCN chambers. *Proceedings of the National Academy of Sciences of the United States of America*, *113*(21), 5828–5834. https://doi.org/10.1073/pnas.1514044113

Saltzman, E. S., De Bruyn, W. J., Lawler, M. J., Marandino, C. A., & McCormick, C. A. (2009). A chemical ionization mass spectrometer for continuous underway shipboard analysis of dimethylsulfide in near-surface seawater. *Ocean Science*, *5*(4), 537–546. https://doi.org/10.5194/os-5-537-2009

Schott, F. A., Xie, S.-P., & McCreary, J. P. (2009). Indian ocean circulation and climate variability. *Reviews of Geophysics*, *47*, RG1002. https://doi.org/10.1029/2007RG000245

Smythe-Wright, D., Boswell, S. M., Lucas, C. H., New, A. L., & Varney, M. S. (2005). Halocarbon and dimethyl sulphide studies around the Mascarene Plateau. *Philosophical Transactions of the Royal Society A: Mathematical, Physical and Engineering Sciences*, *363*(1826), 169–185. https://doi.org/10.1098/rsta.2004.1485

Stohl, A., Forster, C., Frank, A., Seibert, P., & Wotawa, G. (2005). Technical note: The Lagrangian particle dispersion model FLEXPART version 6.2. *Atmospheric Chemistry and Physics*, *5*(9), 2461–2474. https://doi.org/10.5194/acp-5-2461-2005

Stohl, A., & Thomson, D. J. (1999). A density correction for lagrangian particle dispersion models. *Boundary-Layer Meteorology*, *90*(1), 155–167. https://doi.org/10.1023/a:1001741110696

Vallina, S. M., Simo, R., & Gasso, S. (2006). What controls CCN seasonality in the Southern Ocean? A statistical analysis based on satellite-derived chlorophyll and CCN and model-estimated oh radical and rainfall. *Global Biogeochemical Cycles*, *20*, GB1014. https://doi.org/10.1029/2005GB002597

Yin, B., & Min, Q. (2013). Climatology of aerosol optical properties at ACRF sites in the tropical warm pool region. *Journal of Geophysical Research: Atmospheres*, *118*, 2620–2628. https://doi.org/10.1002/jgrd.50234

Yoder, J. A., McClain, C. R., Feldman, G. C., & Esaias, W. E. (1993). Annual cycles of phytoplankton chlorophyll concentrations in the global ocean: A satellite view. *Global Biogeochemical Cycles*, *7*(1), 181–193. https://doi.org/10.1029/93GB02358

Yuan, T., Remer, L. A., & Yu, H. (2011). Microphysical, macrophysical and radiative signatures of volcanic aerosols in trade wind cumulus observed by the A-Train. *Atmospheric Chemistry and Physics*, *11*(14), 7119–7132. https://doi.org/10.5194/acp-11-7119-2011